Impulse control of chaos in the flexible shaft rotating-lifting system of the mono-silicon crystal puller

Zi-Xuan Zhou[1,2], **Celso Grebogi**[1,3], **and Hai-Peng Ren**[1,*]

[1]*Shaanxi Key Laboratory of Complex System Control and Intelligent Information Processing, Xi'an University of Technology, Xi'an, Shaanxi 710048, China*
[2]*School of Computer Science and Engineering, North Minzu University, Yinchuan 750021, Ningxia, China*
[3]*Institute for Complex System and Mathematical Biology, University of Aberdeen AB24 3UE, United Kingdom*

ABSTRACT

Chaos is shown to occur in the flexible shaft rotating-lifting (FSRL) system of the mono-silicon crystal puller. Chaos is, however, harmful for the quality of mono-silicon crystal production. Therefore, it should be suppressed. Many chaos control methods have been proposed theoretically and some have even been used in applications. For a practical plant displaying harmful chaos, engineers from a specified area usually face with the challenge to identifying chaos and to suppressing it by using a proper method. However, despite of the existing methods, chaos control method selection in the FSRL system is not a trivial task. For example, for the OGY method, if one cannot find a practical adjustable parameter, then the OGY method cannot be applied. An impulsive control method is being proposed which is efficiently able to suppress chaos in the FSRL system. The selection of the control parameters is obtained by using the Melnikov method. Simulation results show the correctness of our theoretical analysis and the effectiveness of the proposed chaos control method.

1 Introduction

As a compact dynamics in nonlinear deterministic system with sensitive dependence on initial conditions, chaos started to attract attention after Lorenz analyzed the chaotic dynamics in a weather prediction process [1]. There were lots of chaotic phenomena reported in different fields, for instance, Refs. [2-5]. On one hand, some chaos properties are beneficial in different engineering fields. For example, the ergodicity of chaos is used for optimization algorithms [6], the broad spectrum property for spread spectrum communication [7], electromagnetic noise reduction [8], liquid mixing [9], road roller [10], and soil compactor [11]. The sensitive dependence on initial condition and on parameter are used in secure communication and encryption [12-15], and the Lyapunov spectrum invariance property is used for improving wireless communication performance [16-18]. In this cases, there were some state of art chaos anti-control methods reported to generate chaos from original non-chaotic systems [19-24]. On the other hand, the presence of chaos were reported in industrial plants, such as liquid level control system [25], mill roller system [26], and motor drive system [27], all do compromise the performance of the system. In such cases, chaos need to be suppressed. Since the seminal work of Ott-Grebogi-Yorke on controlling chaos [28], many chaos control methods have been proposed. In general, chaos control methods can be divided into two types according to whether the state feedback is being used. Typical feedback methods include linear state feedback [29], nonlinear state feedback [30] and time-delay feedback [31]; typical chaos control methods without state feedback include periodic perturbation [32] and impulse control [33]. Although there exist many chaos control methods with different features, it is not a trivial task to identify a suitable method to eliminate chaos in a special engineering plant. For example, if the plant has not adjustable parameter, then the OGY method cannot be used. Another example is the avoidance of chaos in a permanent magnet synchronous motor (PMSM), reported in [34]. There are only two variables, i.e., quadrature axis and direct axis stator voltages among three state variables, available for manipulation. Therefore, any control method requiring three manipulated variables regulation will be ineffective to apply to the PMSM system[30].

*Corresponding author. renhaipeng@xaut.edu.cn

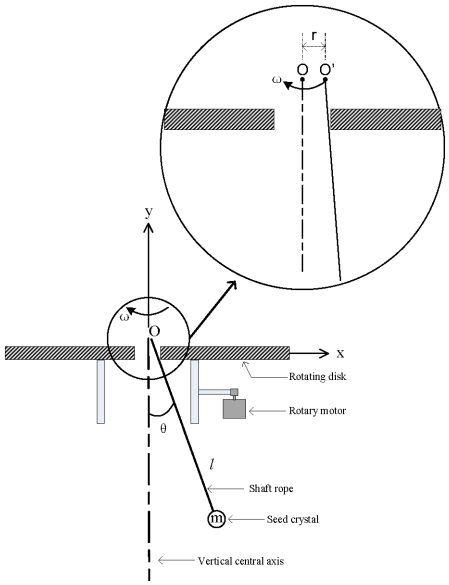

Fig. 1. The simplified schematic diagram of the FSRL system.

Chaotic dynamics in the FSRL system of the crystal puller was unknown until the work in [35], which reported systematically the nonlinear dynamics in the FSRL system. Due to lack of theoretical insight to the chaotic dynamics in the past, engineers tried conventional methods to avoid, what seemed to be a strange phenomenon, by fine manufacturing and mechanical adjustments of some parts of the device, as well as, avoiding the process parameter causing chaotic motion in the crystal producing procedure. However, nonlinear dynamics is an inherent property of the system, and, as such, researchers in the field has to play an active role. Because of our analysis of the FSRL system [35], we find that it is difficult to control or regulate such a practical system, because no manipulated variable can be used and no parameter can be regulated in real time. To solve this problem, we propose an impulse control method to regulate rotation speed of the system intermittently, so as to impose as little impact as possible on the crystal growing process. The controller parameters selection is derived by using the Melnikov method [36].

The remaining of the paper is organized as follows. In section 2, the complex dynamics of the FSRL system is revisited. In section 3, an impulsive control method is proposed specific for chaos control in the FSRL system, and the parameter selection rule is derived using the Melnikov method. The conclusions is given in section 4.

2 System model and the analysis of the controlled system

A simplified schematic diagram of the FSRL system in the crystal seeding stage is given in Fig. 1. In the seeding stage, the crystal seed with 10 mm in diameter is fixed at the end of the systems flexible shaft using a special designed metal clamping device, so that the mass of the total seed and metal can be assumed as a mass point. However, due to the imperfection of the manufacture, the rotating disk might have eccentricity, the actual suspension point O' deviates from the central axis. Under the action of rotation, the eccentric effect causes the periodic perturbation $F(t)$.

The modeling details can be found in [35], we learn that the FSRL system can be treated as a mass point rotating along vertical central axis. Using the Lagrange's equation, the dynamic equation of the FSRL system can be given as:

$$\ddot{\theta} = \frac{r}{l}\omega^2\cos(\omega t) + \omega^2\sin\theta\cos\theta - \frac{g}{l}\sin\theta - \frac{\xi}{m}\dot{\theta}, \tag{1}$$

where θ is the angle (position) between the shaft direction and the rotation center vertical axis, $\dot{\theta}$ (speed) is the time derivative of θ, $\ddot{\theta}$ (acceleration) is the time derivative of $\dot{\theta}$, ω is the rotation speed, l is the length of flexible shaft from the fixed point to the crystal seed, m is the mass of the crystal seed, ξ is the damping coefficient, r is the eccentric distance from the shaft normal point and g is the gravitational acceleration.

Then, let the above equation convert to dimensionless ones and rewrite it as state space equations:

$$\begin{aligned} \dot{x_1} &= x_2 \\ \dot{x_2} &= A\Omega^2\cos(\Omega t) + \Omega^2\sin x_1\cos x_1 - \sin x_1 - cx_2, \end{aligned} \tag{2}$$

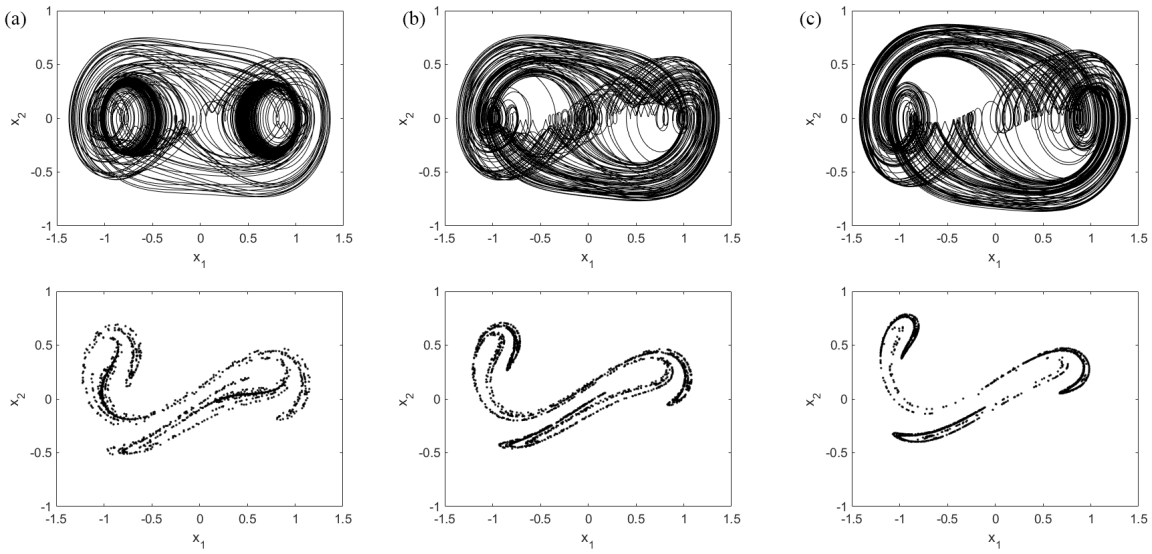

Fig. 2. (a) The phase portrait and the Poincaré section map for $\Omega = 1.2$, $A = 0.16$, and $c = 0.1$ are shown in the upper panel and in the lower panel, respectively. (b) The phase portrait and the Poincaré section map for $\Omega = 1.2$, $A = 0.2$, and $c = 0.15$ are shown in the upper panel and in the lower panel, respectively. (c) The phase portrait and the Poincaré section map for $\Omega = 1.2$, $A = 0.27$, and $c = 0.2$ are shown in the upper panel and in the lower panel, respectively.

where $x_1 = \theta$, $x_2 = \dot{\theta}$, A and Ω are the amplitude and frequency of the external excitations respectively, c is the dimensionless damping constant. It should be noticed that the excitation frequency is consistent with the system rotation speed, which is different from the general parametric pendulum.

System (2) can exhibit various dynamical behaviors, including period doubling bifurcation, symmetry-breaking bifurcation, interior crisis and chaotic motion [35]. Figure 2 shows the phase portrait and the corresponding Poincaré section map for $\Omega = 1.2$ with different A and c. In Fig. 2a, $A = 0.16$, $c = 0.1$, in Fig. 2b, $A = 0.2$, $c = 0.15$, in Fig. 2c, $A = 0.27$, $c = 0.2$. These complex chaotic behaviors are harmful for the quality of mono-silicon crystal production. Therefore, to get rid of this behaviour, we propose an impulsive control to suppress chaos in the FSRL system.

The rotation motor drives the rotating disk through belt pulley, the rotation speed is determined by the crystal growth technique. Therefore, the rotating disk is controlled to work at the appropriate rotation speed through the rotation motor. Due to the special property of the system, there is no state measurement available, no parameter to be tuned (or perturbed), the only manipulated variable is the rotation speed. However, the rotation speed is generally determined by the crystal growth technique, which can not be set as willing. Therefore, the control input should affect the speed as tine as possible. We select rotation speed as control input, and propose impulse control to have tine effect on average rotation speed. we define a positive impulse as speed increasing and a negative impulse as speed decreasing, which is applied the rotation speed Ω.

Considering the working principle of FRSL system, we apply a periodic impulse to Ω, the equation of the controlled system is then given as follow:

$$\begin{aligned} \dot{x_1} &= x_2 \\ \dot{x_2} &= A(P(t))^2 \cos((P(t)) + (P(t))^2 \sin x_1 \cos x_1 \\ &\quad - \sin x_1 - c x_2, \\ P(t) &= \Omega + u(t) \end{aligned} \tag{3}$$

where $u(t)$ is defined as an impulse function with period $T = 2\pi/\Omega$, which is expressed as:

$$u(t) = \sum_{n=0}^{\infty} h(t - nT), \tag{4}$$

with

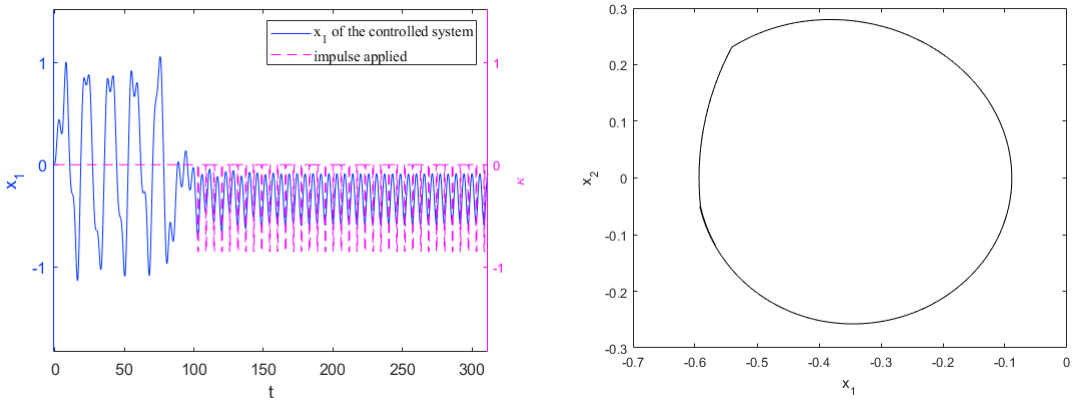

(a) (b)

Fig. 3. (a) The state variable x_1 is plotted with parameters $\Delta = 0.54$ and $\kappa = -0.85$ using blue solid line, magenta dashed line indicates the applied impulse. (b) The corresponding steady state phase portraits after impulse control is activated.

$$h(t) = \begin{cases} \kappa, & -\Delta < t < \Delta \\ 0, & \text{otherwise}, \end{cases} \tag{5}$$

2Δ being the impulse duration and κ is the impulse amplitude. We argued in the next section that the chaotic behavior of the system can be suppressed by a proper design of the above impulse control.

Figure 3a shows state x_1 of system (3) and the impulse applied to the system where $\Omega = 1.1$, $c = 0.1$, and $A = 0.2$, and the impulse control is activated at t=100s. The state variable x_1 is plotted by a blue solid line, the impulse applied is plotted by a magenta dashed line. Figure 3b shows the steady state phase portrait of the system after the impulse control gose into effect. It can be observed that the chaotic motion in the system is suppressed and is replaced by a periodic motion after the proposed impulse control is imposed.

3 Impulse control parameter design using the Melnikov method

In this section, an impulse control method is proposed for suppressing chaos in the crystal seeding stage of the FRSL system. Simulations are performed to validate the effectiveness of the proposed method.

In the following, we present the parameter selection procedure for chaos suppression using impulse control.

Since Δ is small, using $cos(\Omega t)$ as an approximation of $cos(P(t))$, the controlled system equation (3) can be rewritten as:

$$\begin{aligned} \dot{x_1} &= x_2 \\ \dot{x_2} &= A(\Omega + u(t))^2 \cos(\Omega t) + (\Omega + u(t))^2 \sin x_1 \cos x_1 \\ &\quad - \sin x_1 - c x_2, \end{aligned} \tag{6}$$

Theorem 1. For system (3), if the impulse duration Δ and the impulse amplitude κ satisfy the inequality (7), the chaotic behavior is eliminated.

$$\Delta < \frac{\frac{2c}{A} \times \left(\frac{\ln(\sqrt{\alpha^2+1} - \alpha)}{\sqrt{\alpha^2+1}} + \alpha\right) - \pi\Omega^2\Phi(\Omega)}{(2\Omega\kappa + \kappa^2)(\Phi(\Omega) + \Psi(n))}, \tag{7}$$

where

$$\Phi(\Omega) = \sin\left[\frac{\Omega}{\alpha} \sinh^{-1}(\alpha)\right] \times \operatorname{sech}\left(\frac{\Omega\pi}{2\alpha}\right), \tag{8}$$

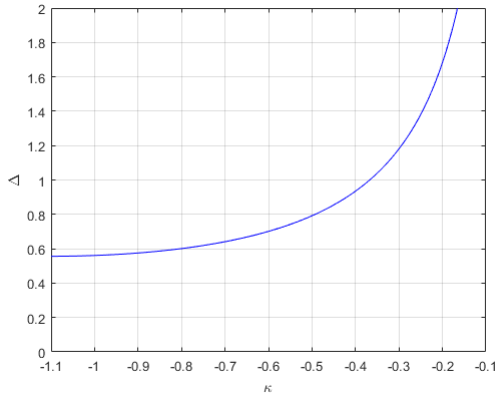

Fig. 4. The pairs of (Δ, κ) above the curve indicated can be used to suppress chaotic motion.

and

$$\Psi(n) = \sum_{n=1}^{N} [(n-1)\sin\frac{\Omega}{\alpha}\sinh^{-1}(\alpha) \times \mathrm{sech}(\frac{\Omega\pi}{2\alpha}(n-1) - (1+n)\sin\frac{\Omega}{\alpha}\sinh^{-1}(\alpha) \times \mathrm{sech}(\frac{\Omega\pi}{2\alpha}(1+n)]. \tag{9}$$

Proof: Let $\Omega t = \tau$; system (3) can be written as:

$$\dot{x} = f(x) + \frac{1}{\Omega} g(x, \tau),$$

where

$$x = \begin{pmatrix} x_1 \\ x_2 \end{pmatrix},$$

$$f(x) = \begin{pmatrix} x_2/\Omega \\ ((\Omega + u(\tau))^2 \sin x_1 \cos x_1 - \sin x_1)/\Omega \end{pmatrix},$$

$$g(x) = \begin{pmatrix} 0 \\ A(\Omega + u(\tau))^2 \cos\tau - c x_2 \end{pmatrix}.$$

The Melnikov function for system (3) is:

$$\begin{aligned} M(\tau) &= \int_{-\infty}^{+\infty} f(q_+^0(\tau)) \wedge g(q_+^0(\tau), \tau + t_0)\, d\tau \\ &= \int_{-\infty}^{+\infty} \frac{x_2^0(\tau)}{\Omega} [A(\Omega + u(\tau + t_0))^2 \cos(\tau + t_0) \\ &\quad - c x_2^0(\tau)]\, d\tau. \end{aligned} \tag{10}$$

Following the mathematical analysis given in the Appendix, we have:

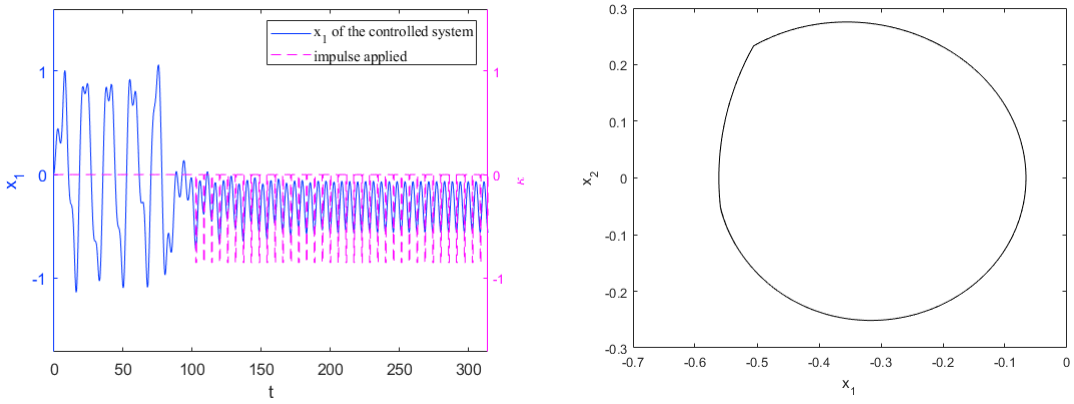

Fig. 5. (a) The state variable x_1 is plotted with parameters $\Delta = 0.57$ and $\kappa = -0.93$ using blue solid line, magenta dashed line indicates the impulse applied; (b) The corresponding steady state phase portrait after impulse control is activated.

$$\begin{aligned} M(t_0) &= A(2\pi\Omega^2 + 4\Omega\kappa\Delta + 2\kappa^2\Delta) \times \Phi(\Omega)\sin(t_0) \\ &+ 2A\sum_{n=1}^{N}(2\Omega\kappa + \kappa^2) \times \psi(n) \\ &- 4c[\frac{\ln(\sqrt{\alpha^2+1}-\alpha)}{\sqrt{\alpha^2+1}} + \alpha]. \end{aligned} \tag{11}$$

where

$$\Phi(\Omega) = \sin[\frac{\Omega}{\alpha}\sinh^{-1}(\alpha)] \times \operatorname{sech}(\frac{\Omega\pi}{2\alpha}), \tag{12}$$

$$\begin{aligned} \psi(n) &= \frac{\sin(n\Delta)}{n}(n-1)\sin\frac{\Omega}{\alpha}\sinh^{-1}(\alpha) \\ &\times \operatorname{sech}(\frac{\Omega\pi}{2\alpha}(1-n)\sin(t_0 - nt_0) \\ &- \frac{\sin(n\Delta)}{n}(1+n)\sin\frac{\Omega}{\alpha}\sinh^{-1}(\alpha) \\ &\times \operatorname{sech}(\frac{\Omega\pi}{2\alpha}(1+n))\sin(t_0 + nt_0), \end{aligned} \tag{13}$$

According the theory in [36], the necessary condition for homoclinic chaos is that $M(t_0)$ is equal to zero. This provides a design criterion for chaos suppression, i.e., if $M(t_0) < 0$ is satisfied for all t_0, then no chaos exists.

Since Δ is small, $\sin(n\Delta)/n \approx \Delta$, $|\sin(t_0)| < 1$, we obtain:

$$\begin{aligned} M(t_0) &< A(2\pi\Omega^2 + 4\Omega\kappa\Delta + 2\kappa^2\Delta) \times \Phi(\Omega) \\ &+ 2A\Delta \times (2\Omega\kappa + \kappa^2)\Psi(n) \\ &- 4c[\frac{\ln(\sqrt{\alpha^2+1}-\alpha)}{\sqrt{\alpha^2+1}} + \alpha] < 0, \end{aligned} \tag{14}$$

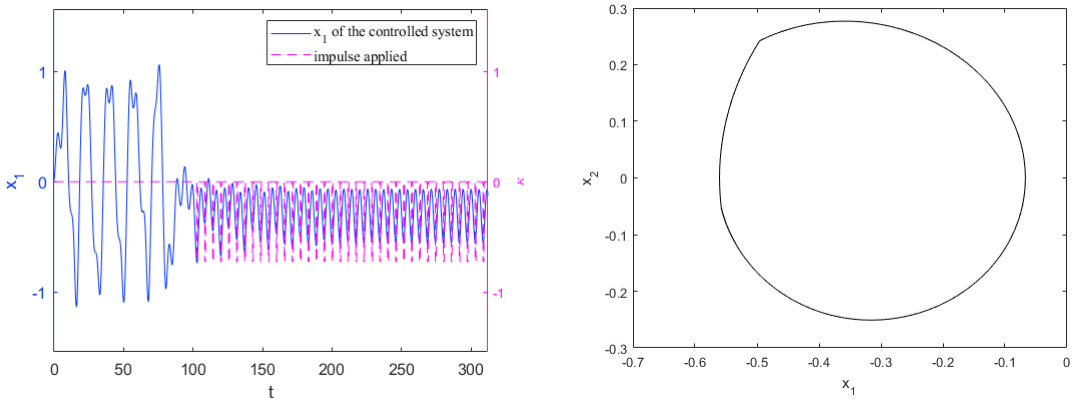

Fig. 6. (a) The state variable x_1 is plotted with parameters $\Delta = 0.63$ and $\kappa = -0.724$ using blue solid line, magenta dashed line indicates the impulse applied; (b) The corresponding steady state phase portrait after impulse control is activated.

where

$$\Psi(n) = \sum_{n=1}^{N} [(n-1)\sin\frac{\Omega}{\alpha}\sinh^{-1}(\alpha) \times \mathrm{sech}(\frac{\Omega\pi}{2\alpha}(n-1) - (1+n)\sin\frac{\Omega}{\alpha}\sinh^{-1}(\alpha) \times \mathrm{sech}(\frac{\Omega\pi}{2\alpha}(1+n)]. \tag{15}$$

Substituting (12) and (15) into (14), we finally get that if:

$$\Delta > \frac{\frac{2c}{A} \times (\frac{\ln(\sqrt{\alpha^2+1}-\alpha)}{\sqrt{\alpha^2+1}} + \alpha) - \pi\Omega^2\Phi(\Omega)}{(2\Omega\kappa+\kappa^2)(\Phi(\Omega)+\Psi(n))} \tag{16}$$

then $M(t_0) < 0$ for all t_0, and chaos is eliminated. The theorem is proved.

The relationship between κ and Δ for chaos suppression is given in Fig. 4, where the system parameters $\Omega = 1.1, c = 0.1$, and $A = 0.2$. Chaos is quenched in the controlled system if the pairs (Δ, κ) are above the curve. The theorem gives us the parameter range to control chaos in FSRL system.

Simulations are carried out to confirm the validity of the criterion given by inequality (16). Choosing the parameter pair $(\Delta, \kappa) = (0.57, -0.93)$ and $(\Delta, \kappa) = (0.63, -0.724)$, when the proposed impulse control is activated at 100s, the simulation results are given in Figs. 5 and 6. Figures 5a and 6a show the state variable x_1, and the corresponding applied impulse. It can be seen that x_1 is stabilized resulting in a periodic state after a transient state after the controller is applied. Figures 5b and 6b depict the corresponding steady state phase portraits, respectively.

4 Conclusions

Chaos in the FSRL system causes defects in the silicon crystal growth quality, which need to be avoided. Therefore in this paper, the Melnikov method is used to suppress the chaotic dynamical behaviour. An impulse control is proposed to eliminate chaos. We also derive the parameter selection rule for impulse control to suppress chaos using the Melnikov method. We have found that the impulse control is simple, not requiring state feedback, and it is an effective control technique to control chaos in the FSRL system.

Acknowledgements

This work has been supported by the Key Program of National Natural Science Foundation of China (Grant No.61533014).

References

[1] Lorenz, E. N.: Deterministic nonperiodic flow. Journal of the atmospheric sciences. 20(2), 130-141 (1963).

[2] Wang Y., Yang R., Zhang B., Hu, W.: Smale horseshoes and symbolic dynamics in the buck-boost DC-DC converter. IEEE Transactions on Industrial Electronics. 65(1), 800-809 (2017).

[3] Maciver, B., Bland, B. H.: Chaos analysis of EEG during isoflurane-induced loss of righting in rats. Frontiers in systems neuroscience. 8(203), 1-8 (2014).

[4] Chvez, J. P., Pavlovskaia, E., Wiercigroch, M.: Bifurcation analysis of a piecewise-linear impact oscillator with drift. Nonlinear Dynamics. 77(1-2), 213-227 (2014).

[5] Nayfeh, A. H., Harb, A. M., Chin, C. M.: Bifurcations in a power system model. International Journal of Bifurcation & Chaos. 6(03), 497-512 (1996).

[6] Liu, W. B., Luo, N. S., Pan, G., Aijia, O.: Chaos Particle Swarm Optimization Algorithm for Optimization Problems. International Journal of Pattern Recognition and Artificial Intelligence. 32(11), 1859019 (2018).

[7] Xu, W. K., Wang, L., Kolumbán, G.: A new data rate adaption communications scheme for code-shifted differential chaos shift keying modulation. International Journal of Bifurcation & Chaos. 22(08): 1527-92 (2012).

[8] Li, H. G., Gong, S. D., Liu, J. W., Su, D. L.: CMOS-Based Chaotic PWM Generator for EMI Reduction. IEEE Transactions on Electromagnetic Compatibility. 59(4), 1224-1231 (2017).

[9] Solomon, T. H., Mezić, I.: Uniform resonant chaotic mixing in fluid flows. Nature. 425(6956), 376-380 (2003).

[10] Ren, H. P., Han, C. Z.: Chaotifying control of permanent magnet synchronous motor. 2006 CES/IEEE 5th International Power Electronics and Motion Control Conference. IEEE, 1: 1-5 (2006).

[11] Ren, H. P., A single direction chaotic speed generation method based on PMSM, American Patent, US10236811 B2, 19 Mar 2019.

[12] Pérez-Resa, A., Garcia-Bosque, M., Sánchez-Azqueta, C., Celma, S.: Chaotic Encryption Applied to Optical Ethernet in Industrial Control Systems. IEEE Transactions on Instrumentation and Measurement. 68(12), 2896550 (2019).

[13] Ren, H. P., Bai, C., Tian, K., Grebogi, C.: Dynamics of delay induced composite multi-scroll attractor and its application in encryption. International Journal of Non-Linear Mechanics, 2017, 94: 334-342.

[14] Ren, H. P., Bai, C., Huang, Z. Z., Grebogi, C.: Secure communication based on hyperchaotic Chen system with time-delay. International Journal of Bifurcation & Chaos. 27(05), 1750076 (2017).

[15] Wang, X. Y., Wang, Q.: A fast image encryption algorithm based on only blocks in cipher text. Chinese physics B. 23(3): 030503 (2014).

[16] Ren, H. P., Baptista, M. S., Grebogi, C.: Wireless Communication with Chaos. Physical Review Letters, 2013, 110(18):184101.

[17] Yao, J. L., Li, C., Ren, H. P., Grebogi, C.: Chaos-based wireless communication resisting multipath effects. Physical Review E. 96(3): 032226 (2017).

[18] Yao, J. L., Sun, Y. Z., Ren, H. P., Grebogi, C.: Experimental wireless communication using chaotic baseband waveform. IEEE Transactions on Vehicular Technology. 68(1): 578-591 (2018).

[19] Chen G., Lai D.: Feedback Anticontrol of Discrete Chaos. International Journal of Bifurcation & Chaos. 08(07):1585-1590 (1998).

[20] Wang X. F., Chen G., Yu X.: Anticontrol of chaos in continuous-time systems via time-delay feedback. Chaos. 10(4): 771-779 (2000).

[21] Ren H. P., Liu D., Han C. Z.: Anticontrol of chaos via direct time delay feedback. Acta Physica Sinica. 55(6): 2694C2701 (2006).

[22] Wang Z., Chau K. T.: Anti-control of chaos of a permanent magnet DC motor system for vibratory compactors. Chaos Solitons & Fractals. 36(3):694-708 (2008).

[23] Moreno-Valenzuela J.: Adaptive anti control of chaos for robot manipulators with experimental evaluations. Communications in Nonlinear ence and Numerical Simulation. 18(1):1-11 (2013).

[24] Moreno-Valenzuela J., Carlos Torres-Torres C.: Adaptive chaotification of robot manipulators via neural networks with experimental evaluations. Neurocomputing. 182:56-65 (2016).

[25] Cai, Y., Liu, W., Wang, Z.: Optimal control of chaotic motions in the liquid level regulation system. Control Theory and Applications. 16(2): 258-261 (1999).

[26] Liao, M., Su, Y., Zhou, Y.: Oscillation Reconstruction and Bifurcation Analysis of a Drillbit-Rock Vibro-Impact System. International Journal of Bifurcation & Chaos, 27(01): 1750013 (2017).

[27] Tahir, F. R., Abdulhassan, K. M., Abdullah, M. A., Pham, V. T., Hoang, T. M., Xiong, W.: Analysis and Stabilization of Chaos in Permanent Magnet DC Motor Driver. International Journal of Bifurcation & Chaos. 27(11), 1750173 (2017).

[28] Ott, E., Grebogi, C., Yorke, J.: Controlling chaos. Physical Review Letters. 64(11), 1196-1199 (1990).

[29] Chen, G. R., Dong, X. N.: On feedback control of chaotic nonlinear dynamic systems. International Journal of Bifurcation & Chaos. 02(02), 407-411 (1992).

[30] Ren, H. P., Liu, D. Nonlinear feedback control of permanent magnet synchronous motor, IEEE Transactions on Circuits and System II. 51(1), 45-50 (2006).

[31] Pyragas, K.: Continuous control of chaos by self-controlling feedback. Physics Letters A. 170, 421C8 (1992).
[32] Wang, X., Wang, M.: Chaotic control of Liu system with periodic parametric perturbations. International Journal of Modern Physics B. 25(22), 3011-3017 (2001).
[33] Yang, T., Yang, L. B., Yang, C. M.: Impulsive control of Lorenz system. Physica D. 110(1-2), 18-24 (1997).
[34] Li, Z., Park, J. B., Joo, Y. H., Zhang, B., Chen, G. R.: Bifurcations and chaos in a permanent-magnet synchronous motor. IEEE Transactions on Circuits and Systems I: Fundamental Theory and Applications. 49(3), 383-387 (2002).
[35] Ren, H. P., Zhou, Z. X., Grebogi, C.: Nonlinear dynamics in the flexible shaft rotating-lifting system of silicon crystal puller using Czochralski method. Nonlinear Dynamics. DOI: 10.1007/s11071-020-05592-9, (2020).
[36] Melnikov, V.K.: On the stability of the center for time periodic perturbations. Transactions of the Moscow Mathematical Society. 12: 3-52 (1963).

Appendix

In this appendix, the calculation of the Melnikovs function (11) is carried out. Recalling (10) as follows:

$$\begin{aligned} M(\tau) &= \int_{-\infty}^{+\infty} \frac{x_2(\tau)}{\Omega}[A(\Omega+u(\tau+t_0))^2\cos(\tau+t_0) \\ &\quad - cx_2(\tau)]\,d\tau \\ &= \int_{-\infty}^{+\infty} \frac{1}{\Omega}\times\frac{-2\alpha^2\sinh(\alpha\tau\setminus\Omega)}{\alpha^2+\cosh^2(\alpha\tau\setminus\Omega)}[A(\Omega+u(\tau+t_0))^2 \\ &\quad \times\cos(\tau+t_0) - c\frac{-2\alpha^2\sinh(\alpha\tau\setminus\Omega)}{\alpha^2+\cosh^2(\alpha\tau\setminus\Omega)}]\,d\tau \end{aligned}$$

$P(t)=(\Omega+u(t))^2$ is also a periodic signal and it can be represented in terms of the Fourier series $P_N(t)$,

$$\begin{aligned} P_N(t) &= (\Omega^2+\frac{2\Omega\kappa\Delta}{\pi}+\frac{\kappa^2\Delta}{\pi}) \\ &\quad +\sum_{n=1}^{N}(\frac{4\Omega\kappa}{n\pi}+\frac{2\kappa^2}{n\pi})\sin(n\Delta)\cos(n\tau) \end{aligned} \tag{A1}$$

As indicated in [36], the two homoclinic orbits for the unperturbed system of (2) are already obtained,

$$q_+^0(t) = (2\cot^{-1}(\frac{1}{\alpha})\cosh\alpha t, -\frac{2\alpha^2\sinh\alpha t}{\alpha^2+\cosh^2\alpha t}),$$

and

$$q_-^0(t) = (-2\cot^{-1}(\frac{1}{\alpha})\cosh\alpha t, \frac{2\alpha^2\sinh\alpha t}{\alpha^2+\cosh^2\alpha t}).$$

with $q_+^0(t)$, (10) becomes (A2)(in next page),
where

$$\Phi(\Omega) = \sin[\frac{\Omega}{\alpha}\sinh^{-1}(\alpha)]\times\operatorname{sech}(\frac{\Omega\pi}{2\alpha}),$$

and

$$\psi(n) = \frac{\sin(n\Delta)}{n}(n-1)\sin\frac{\Omega}{\alpha}\sinh^{-1}(\alpha) \times \operatorname{sech}(\frac{\Omega\pi}{2\alpha}(1-n)\sin(t_0 - nt_0) - \frac{\sin(n\Delta)}{n}(1+n)\sin\frac{\Omega}{\alpha}\sinh^{-1}(\alpha) \times \operatorname{sech}(\frac{\Omega\pi}{2\alpha}(1+n))\sin(t_0+nt_0),$$

By this way, we can derive Eq. (11).
The derivation for $q_-^0(t)$ can be derived in the same way.

$$\begin{aligned}
M(t_0) &= \int_{-\infty}^{+\infty}\frac{1}{\Omega}\times\frac{-2\alpha^2\sinh(\alpha\tau\setminus\Omega)}{\alpha^2+\cosh^2(\alpha\tau\setminus\Omega)}[A(\Omega^2+\frac{2\Omega\kappa\Delta}{\pi}+\frac{\kappa^2\Delta}{\pi})+\sum_{n=1}^{N}(\frac{4\Omega\kappa}{n\pi}+\frac{2\kappa^2}{n\pi})\sin(n\Delta)\cos(n\tau))\cos(\tau+t_0) \\
&- c\frac{-2\alpha^2\sinh(\alpha\tau\setminus\Omega)}{\alpha^2+\cosh^2(\alpha\tau\setminus\Omega)}]\,d\tau \\
&= A(\Omega^2+\frac{2\Omega\kappa\Delta}{\pi}+\frac{\kappa^2\Delta}{\pi})\int_{-\infty}^{+\infty}\frac{1}{\Omega}\times\frac{-2\alpha^2\sinh(\alpha\tau\setminus\Omega)}{\alpha^2+\cosh^2(\alpha\tau\setminus\Omega)}\cos(\tau+t_0)\,d\tau \\
&+ A\sum_{n=1}^{N}(\frac{4\Omega\kappa}{n\pi}+\frac{2\kappa^2}{n\pi})\sin(n\Delta)\int_{-\infty}^{+\infty}\frac{1}{\Omega}\times\frac{-2\alpha^2\sinh(\alpha\tau\setminus\Omega)}{\alpha^2+\cosh^2(\alpha\tau\setminus\Omega)}\cos(n\tau)\cos(\tau+t_0)\,d\tau \\
&- c\int_{-\infty}^{+\infty}\frac{1}{\Omega}\times(\frac{-2\alpha^2\sinh(\alpha\tau\setminus\Omega)}{\alpha^2+\cosh^2(\alpha\tau\setminus\Omega)})^2\,d\tau \\
&= A(\Omega^2+\frac{2\Omega\kappa\Delta}{\pi}+\frac{\kappa^2\Delta}{\pi})\times 2\pi\sin(\frac{\Omega}{\alpha}sinh^{-1}(\alpha))sech(\frac{\pi\Omega}{2\alpha})sin(t_0) \\
&+ A\sum_{n=1}^{N}(\frac{4\Omega\kappa}{n\pi}+\frac{2\kappa^2}{n\pi})\sin(n\Delta)\int_{-\infty}^{+\infty}\frac{1}{\Omega}\times\frac{-2\alpha^2\sinh(\alpha\tau\setminus\Omega)}{\alpha^2+\cosh^2(\alpha\tau\setminus\Omega)}[cos(n(\tau+t_0)+(\tau+t_0)) \\
&+ cos(n(\tau+t_0)-(\tau+t_0))]\,d\tau \\
&- 4c(\frac{\ln(\sqrt{\alpha^2+1}-\alpha)}{\sqrt{\alpha^2+1}}+\alpha) \\
&= A(\Omega^2+\frac{2\Omega\kappa\Delta}{\pi}+\frac{\kappa^2\Delta}{\pi})\times 2\pi\sin(\frac{\Omega}{\alpha}sinh^{-1}(\alpha))sech(\frac{\pi\Omega}{2\alpha})sin(t_0) \\
&+ A\sum_{n=1}^{N}(\frac{4\Omega\kappa}{n\pi}+\frac{2\kappa^2}{n\pi})\sin(n\Delta)\pi(n-1)\sin(\frac{\Omega}{\alpha}sinh^{-1}(\alpha))sech(\frac{\pi\Omega}{2\alpha}(n-1))sin((n-1)t_0) \\
&- A\sum_{n=1}^{N}(\frac{4\Omega\kappa}{n\pi}+\frac{2\kappa^2}{n\pi})\sin(n\Delta)\pi(n+1)\sin(\frac{\Omega}{\alpha}sinh^{-1}(\alpha))sech(\frac{\pi\Omega}{2\alpha}(n+1))sin((n+1)t_0) \\
&- 4c(\frac{\ln(\sqrt{\alpha^2+1}-\alpha)}{\sqrt{\alpha^2+1}}+\alpha) \\
&= A(2\pi\Omega^2+4\Omega\kappa\Delta+2\kappa^2\Delta)\times\Phi(\Omega)\sin(t_0)+2A\sum_{n=1}^{N}(2\Omega\kappa+\kappa^2)\times\psi(n)-4c[\frac{\ln(\sqrt{\alpha^2+1}-\alpha)}{\sqrt{\alpha^2+1}}+\alpha].
\end{aligned} \tag{A2}$$